Wake field study of tidal turbines under realistic flow conditions

Jérôme Thiebot, Nicolas Guillou, Sylvain Guillou, Andrew Good, Michael Lewis

Wake field study of tidal turbines under realistic flow conditions

Jérôme Thiébot[1], Nicolas Guillou[2], Sylvain Guillou [1], Andrew Good[3,4], Michael Lewis[4]

1. Normandie Univ, UNICAEN, LUSAC, 60 rue Max Pol Fouchet, CS 20082, 50130 Cherbourg-Octeville, France

2. Cerema, Laboratoire de Génie Côtier et Environnement, ER, 155 rue Pierre Bouguer, Technopôle Brest-Iroise, BP 5, 29280 Plouzané, France

3. BrightWind Limited, Ireland

4. OpenHydro Group Limited, 1 Custom House Plaza, Harbourmaster place, IFSC, Dublin 1, Ireland

jerome.thiebot@unicaen.fr ; nicolas.guillou@cerema.fr ; sylvain.guillou@unicaen.fr ; andrew@brightwindanalysis.com ; michael.lewis@xocean.com

Abstract— **Numerical modelling of the flow interactions between tidal turbines in arrays is a prerequisite to assess the energy production potential and to optimise the layout of tidal stream energy farms. It requires (i) a refined representation of the tide propagation and (ii) a reliable estimate of the flow characteristics around the turbines. The Actuator Disk (AD) theory is recognised as a reliable parameterisation to approach the far wake of fixed horizontal-axis turbines and was therefore implemented to provide recommendations as regards to the design of arrays, especially the optimal spacing between devices. However, analysis of the arrangement of tidal stream turbines are typically restricted to schematic test cases with idealised bathymetry and inflow conditions. The present study aims to investigate the flow interactions between turbines in a stream energy site with spatially- and time-varying tidal conditions. The site of application is the Alderney Race (English Channel), an area with strong potential for the exploitation of tidal energy in European shelf seas. The three-dimensional numerical model Telemac3D is used to capture the flow at both the regional and the array scales. Predictions are first assessed against ADCP measurements acquired around the island of Alderney. A series of simulations, representing turbines with the AD theory, are then performed to investigate the influence of the wake interactions on the energy production of individual devices. In those simulations, the turbines are represented with the AD theory. The zone occupied by the turbines is 20D-long and 15D-wide (D is the turbine diameter). Different layouts (isolated, aligned and staggered turbines) and different longitudinal and lateral spacings are considered to investigate the effect of the turbines' arrangement and density on the array energy production. The results show that, for a given turbines density within the array, the staggered layout produces more than the aligned layout (+16 %). When the turbines are staggered, a minimal lateral spacing of 5D is required to avoid wake overlapping. However, when the turbines are aligned, the lateral spacing has a small influence on the turbines production. It is therefore possible to pack the turbines close to each other in the lateral direction. The simulations also outline that the turbulence develops much faster within the array when the turbines are aligned.**

Keywords— **Numerical modelling, Tidal turbine, Actuator Disk theory, Telemac, Alderney Race**

I. INTRODUCTION

A significant part of the worldwide tidal energy resource is found in restricted areas - predominantly in the vicinity of headlands and straits that accelerate the currents (Neill *et al.*, 2016). However, the installation of tidal-stream turbines within those locations is subjected to environmental and practical constraints including an intense vessel traffic, a limited water depth and an irregular seabed topography. As the tidal turbines can be installed in zones that are limited in surface areas, it is necessary to arrange the devices so that they maximise the energy production. An efficient design of tidal farm is also useful to reduce the number of turbines required to reach a targeted output and has thus significant impacts on the construction, installation and maintenance costs. In the last few years, numerous approaches have been developed to understand how turbines' layout within a farm influences the total power output. Vennell *et al.* (2015) reviewed those issues in optimising the tidal array arrangement focusing on both (i) the macro-design maximising the farm-efficiency with an optimal number of devices and (ii) the micro-design boosting the array energy output by adjusting individual turbines' position.

The efficiency of tidal farms was investigated with analytical models considering different arrangements: (i) fences of turbines regularly arrayed across the entire channel cross-section (Garrett and Cummins, 2007), (ii) fences of turbines partially blocking a channel (Nishino and Willden, 2013) and (iii) two rows of staggered and aligned turbines (Draper and Nishino, 2014). Such models provided further insights about the processes controlling the turbines' output exhibiting, in particular (i) the flow diversion caused by the blockage effect, (ii) the length of the mixing region behind rows and (iii) the length required for pressure equalisation. However, these analytical models considered highly idealised upstream flow conditions and they neglected the three-dimensional (3D) effects and the influence of the turbulence on the flow recovery. The efficiency of multiple turbines was thus investigated with scaled turbines deployed in experimental flumes. Flow-interactions between turbines were thereby investigated considering (i) two turbines (Mycek *et al.*, 2014), (ii) groups of up to ten turbines (Stallard *et al.*, 2013) and (iii) multiple rows of turbines (Coles *et al.*, 2016). These experiments aimed at investigating the structure of the wakes and at analysing how it affected the performance of individual turbines. Unfortunately, these experiments were not fully representative of full-scale tidal turbines as the Reynolds similarity was not established. Complementing analytical and experimental research studies, numerical modelling is often retained to perform wake field studies of tidal current turbines, providing further fundamental insights to optimise the layout of devices within the array.

Numerous numerical approaches can be implemented to represent tidal-stream turbines. The most sophisticated models rely on blade resolved Computational Fluid Dynamics (CFD) (*e.g.*, Ahmed *et al.*, 2017) and are commonly applied to compute the turbine loading and assess the power coefficients. Although such models provide an accurate description of the flow in the vicinity of the turbine, the great associated CPU cost prevents simulating the flow through an array of devices. Computing larger time and spatial scales requires thus simpler turbine models such as the Actuator line or Blade Element Momentum methods coupled to CFD. Relying on such approaches, multiple turbines were thereby simulated to analyse the wake interactions between several rows of devices and assess the influence of devices' layout on the power production (Bai *et al.*, 2013, Churchfield *et al.*, 2013, Malki *et al.*, 2014). Although such applications provide further insights about tidal stream configuration to optimise output power, the inflow conditions are generally highly idealised (stationary velocity, inflow parallel to the turbines' axis), and only a limited number of inflow configurations can be tested and compared. The application of such approaches to investigate how the tidal stream turbines deployed at a given site interact with each other during a tidal cycle is thus not straightforward.

The Actuator Disks (AD) theory is a simpler method to simulate the turbine effect within an array. It consists in representing the energy extraction of a horizontal-axis turbine by imposing a pressure drop in the area swept by the blades. In practice, the force (thrust) being applied in the disk is imposed *via* a momentum sink into the Reynolds Averaged Navier Stokes (RANS) equations. Contrarily to more sophisticated turbine representation, the AD approach can easily be implemented in regional hydrodynamic models (Peyrard *et al.*, 2006, Roc *et al.*, 2013, Abolghasemi *et al.*, 2016, Thiebot *et al.*, 2016, Goward Brown *et al.*, 2017). Considering several tidal energy sites, AD were thereby used to assess the perturbations induced by turbines on the hydrodynamics and the sediment transport (*e.g.*, Fallon *et al.*, 2014, Goward Brown *et al.*, 2017, O'Hara Murray and Gallego, 2017). Yang *et al.* (2013, 2014) also implemented a similar approach to investigate the effect of both the array arrangement and the density of turbines on the energy extraction. Those applications, focusing on real-world sites, are most of the time performed in large computational domains with spatial resolutions of the same order of turbines' diameters. In this context (large-scale applications with coarse mesh), the AD approach is applied to extract from the flow a given amount of energy (representative of the turbines' thrust). However, the flow representation in the vicinity of the turbines is crude as the geometry of the devices is not reproduced and the spatial resolution is too coarse to correctly approach wakes' interactions. Another type of application consists in using AD to simulate the flow at the array scale. Whereas these simulations require a much greater spatial resolution than in the aforementioned regional applications, the AD approach provides reasonable predictions in the far wake of devices (over five turbine's diameters from the disk) and in the flow bypass around the turbines (Batten *et al.*, 2013, Liu *et al.*, 2016). AD can therefore be applied to design arrays provided that (i) a high spatial resolution is used in the vicinity of devices and (ii) that the turbulence model is able to mimic the effect of the unresolved small-scale processes (Nguyen *et al.*, 2016, Shives and Crawford, 2017).

Despite the ability of the AD-RANS approach to capture both the regional and the array scales, wake field studies with AD typically consider schematic configurations with uniform bathymetry (Nguyen *et al.*, 2017, 2019) and regular coastlines (Roc *et al.*, 2014), and steady unidirectional inflow conditions (Liu *et al.*, 2016). The present investigation aims at performing a numerical wake field study under spatially- and time-varying tidal hydrodynamic conditions in a planned stream energy site. The approach relies on the three-dimensional model Telemac3D (Hervouet, 2007) in which the energy extraction is simulated with high resolution AD. By capturing both the regional and the array scales, the model provides a refined estimate of the energy production of individual devices. The numerical method is applied to hypothetical arrays of turbines located in the Alderney Race (Figure 1). This site is located in the Northwest European shelf seas, in the English Channel, between the island of Alderney and the cape of La Hague, France. With a maximum upper bound for power extraction of 5.1GW (Coles *et al.*, 2017), it is one of the most promising site for tidal energy exploitation in Western Europe.

Regional model performances, without turbines, are first assessed against available ADCP measurements around the Alderney Island (section II). The method for analysing the wake-field is then presented focusing on (i) the turbine parameterisation in the 3D model, (ii) the scenarios for tidal energy extraction and (iii) the metrics for the assessment of the tidal farm production (section III). The simulations of the flow through several arrays of turbines deployed in the Alderney Race are finally analysed to investigate the effects of the type of layout (staggered or aligned) and the turbine density on the individual and global production of devices (section IV).

A. *Model configuration*

Telemac3D solves the free-surface unsteady RANS equations using a finite element method (Weilbeer and Jankowski, 1999, Hervouet, 2007). Different model configurations are possible. Here, the turbulence is modelled with a two-equations k-ε closure scheme assuming an isotropic turbulence hypothesis. The non-hydrostatic set of equations is retained. Using the non-hydrostatic set of equations is not necessary for simulating environmental flows and, in addition, it requires a greater computational cost than the hydrostatic set of equations (here, the extra cost is 88%). However, for modelling the flow around turbines, Thiébot *et al.* (2016) have shown that it significantly improves the results. In this contribution, the regional and the array scales are resolved. For consistency, we thus use the non-hydrostatic set of equations for both the regional model validation (agreement with ADCP, section II.B) and the wake-field study (sections III and IV). The continuity and momentum equations take the following form:

$$\frac{\partial u}{\partial x}+\frac{\partial v}{\partial y}+\frac{\partial w}{\partial z}=0 \quad (1)$$

$$\begin{cases} \frac{\partial u}{\partial t}+u\frac{\partial u}{\partial x}+v\frac{\partial u}{\partial y}+w\frac{\partial u}{\partial z}=\frac{-1}{\rho}\frac{\partial p}{\partial x}+\nu\Delta u+f_x \\ \frac{\partial v}{\partial t}+u\frac{\partial v}{\partial x}+v\frac{\partial v}{\partial y}+w\frac{\partial v}{\partial z}=\frac{-1}{\rho}\frac{\partial p}{\partial y}+\nu\Delta v+f_y \\ \frac{\partial w}{\partial t}+u\frac{\partial w}{\partial x}+v\frac{\partial w}{\partial y}+w\frac{\partial w}{\partial z}=\frac{-1}{\rho}\frac{\partial p}{\partial z}-g+\nu\Delta w+f_z \end{cases} \quad (2)$$

where x and y are the geographic coordinates, z is the vertical coordinate, u, v and w are the three components of the velocity field, t is the time, g is the gravity acceleration (g = 9.81 m/s^2), ν is the kinematic viscosity (molecular and turbulent viscosities), f_x, f_y and f_z are the source terms (bottom friction, Coriolis force and action of the turbines) and ρ is the water density (ρ = 1025 kg/m^3).

The computational domain covers the English Channel (Figure 1). The mesh density was imposed using four zones with decreasing cell sizes: (i) 10 km – 500 m in zone n°1, (ii) 500 m – 200 m in zone n°2, (iii) 200 m – 100 m in zone n°3 and (iv) 100 m (uniform cell size) in zone n°4 (Figure 1). The minimum cell size (100 m in zone n°4) has been chosen from the results of a sensitivity study, which indicated that using twice-smaller cell size (50 m) did not improve the model performance significantly. The horizontal mesh contains 240,807 nodes and the domain is discretised vertically using 40 equally-spaced horizontal planes (sigma-transformation). The choice of the number of layers was dictated by the resolution of the AD (discussed in section III.C) rather than by considerations on the regional model performance. The 3D mesh therefore contains 9,632,280 nodes. The bathymetric data derives from a Digital Elevation Model (DEM) provided by the SHOM ("Service Hydrographique et Océanographique de la Marine) (2015) with a spatial resolution of 111 m. The model time step is set to 10 s. Tidal conditions along the Western and Northern sea boundaries are provided by the TPXO European Shelf 2008 database (Egbert *et al.*, 2010). It uses 11 tidal constituents (M2, S2, N2, K2, K1, O1, P1, Q1, M4, MS4, MN4). The bottom shear stress $\overrightarrow{\tau_b}$ is computed with the following quadratic friction law:

$$\overrightarrow{\tau_b}=\rho C_b\|\vec{U}\|\vec{U} \quad (3)$$

$$C_b=\left(\frac{\kappa}{ln(H/ez_0)}\right)^2 \quad (4)$$

where $\|\vec{U}\|$ is the magnitude of the depth-averaged horizontal current, $C_b$is the friction coefficient, $\kappa = 0.4$ is the von Karman constant, H is the water depth and z_0 is the bottom roughness defined as the height above the seabed where the fluid velocity is nil. The roughness parameterisation is based on four types of seabed: (i) sands, (ii) gravels, (iii) pebbles and rock outcrops and (iv) rocks. The mapping of seabed types is based on a sedimentological cartography established by SHOM (2018) (Figure 2). For the sands and the gravels, the roughness parameter is set to z_0 = 0.4 mm and 3 mm, respectively. Those values come from the observations compiled by Soulsby (1983). For the two other types of seabed (pebbles and rock outcrops and rocks), a sensitivity analysis was performed using a methodology comparable to Guillou and Thiébot (2016). It consisted in testing different values of roughness and in choosing those that provided the best fit between model predictions and ADCP observations. By so doing, we obtained z_0 = 10 mm for pebbles and rock outcrops and 20 mm for rocks.

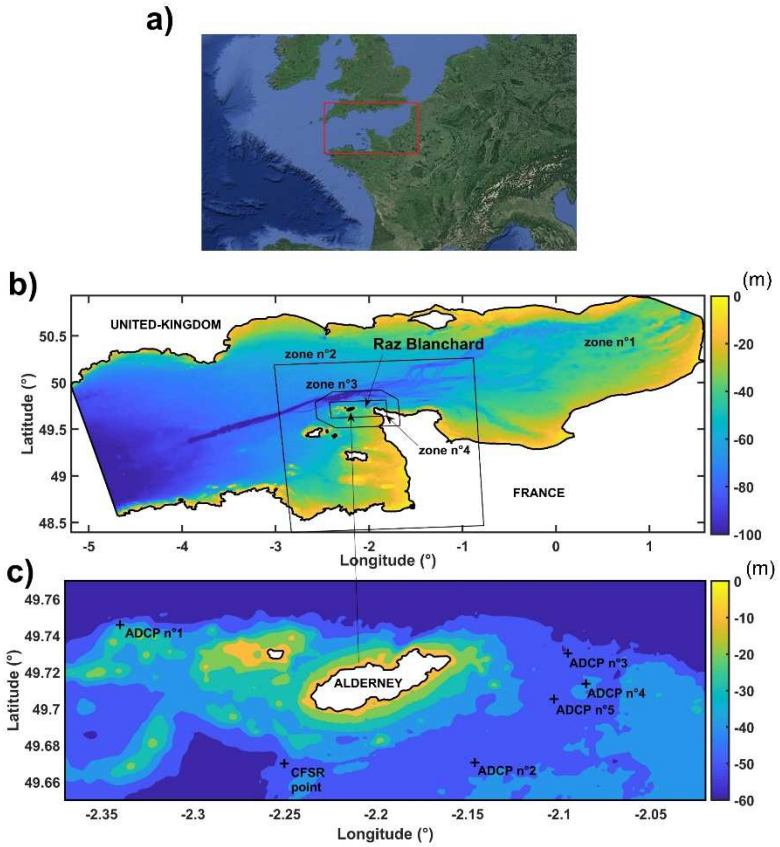

Figure 1: a) Location of the study zone. b) English Channel model domain and bathymetry (with respect to the mean sea level). The four zones (n°1-4) indicate the different mesh densities. c) Locations of the ADCP used for the model validation.

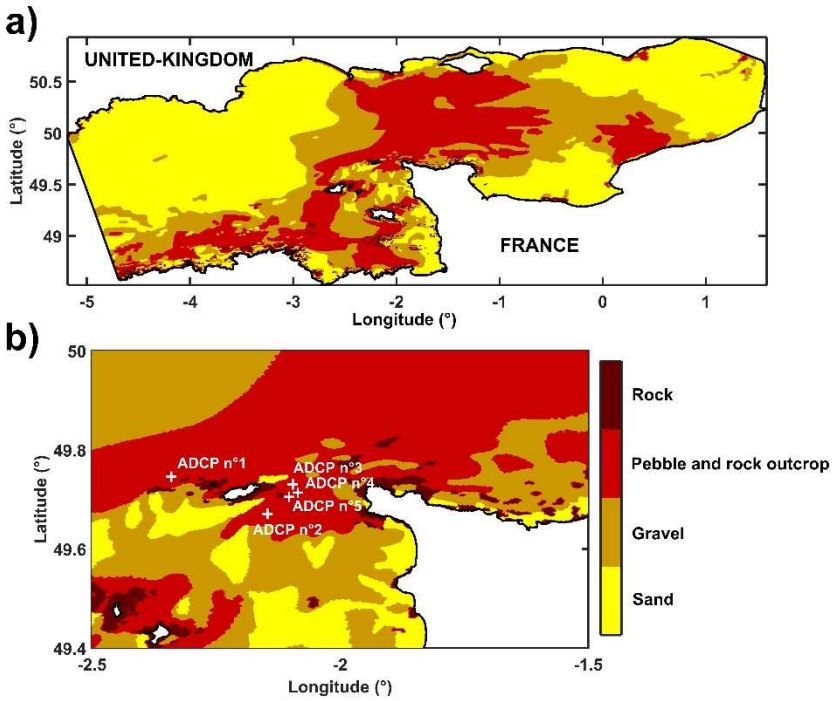

Figure 2: Sediment bottom types at the scale of the English Channel with a detailed view in the Alderney Race.

B. Evaluation of model predictions

The hydrodynamic model of the Alderney Race is assessed against ADCP measurements provided by the company OpenHydro. This dataset gathers measurements acquired by five ADCPs deployed simultaneously around the Alderney Island (Figure 1 and Table 1). The height of the vertical cells is 2 m and the ADCP sampling frequency is 1 Hz. The validation period covers six days with contrasting tidal conditions. It extends from August, the 6th in 2014 at 00:00 (UT) to August, the 12th at 00:00 (UT). The model is run 24 h before the beginning of the validation period to allow the model to spin up from the initial conditions (current velocity and free surface elevation) given by the TPXO database. The meteorological forcing (wind and pressure) and the wave effect are not integrated assuming that the hydrodynamics of the Alderney Race is mostly controlled by the tide (Thiébot *et al.*, 2015). This assumption is reinforced regarding the available meteo-oceanographic data during the measurement period. The CFSR database (Saha *et al.*, 2010) shows thus that the met-ocean conditions were calm during the validation period. At the point of coordinates (2.25°W; 49.67°N) located in 44 m depth (CFSR point in Figure 1), the mean significant wave height remains thus smaller than 1 m during the first four days of the validation period and exceeds 2 m during the last two days with a peak value of 2.85 m during August, the 10th. As regards the wind speed, it fluctuates around 5 m/s during the first four days and exceeds 10 m/s during the last two days.

Table 1: Location and depth of the ADCPs. Water depths refer to the mean sea level.

ADCP n°	Latitude	Longitude	Depth (m)
1	49.746	-2.340	34.1
2	49.671	-2.146	43.7
3	49.730	-2.095	48.2
4	49.714	-2.085	40.4
5	49.705	-2.103	44.1

To obtain quantities comparable to the model results (the model computes Reynolds-averaged values), the ADCP signal is filtered using a moving average. The velocity at the time *t* is thus calculated as the mean velocity over the period [*t*-30 s; *t*+30 s]. The model validation is based on the magnitude and direction of the horizontal velocities and the power density (taken equal to $0.5\rho\|\vec{u}\|^3$ where $\|\vec{u}\|$ is the horizontal velocity magnitude). Statistical parameters used for the assessment of model's predictions are the root mean square error RMSE, the bias B, the relative bias RB and the index of agreement IA (Eqs.5-8).

$$RMSE = \sqrt{\frac{1}{N}\sum_{i=1}^{i=N}(mod_i - mes_i)^2} \quad (5)$$

$$B = \overline{mod} - \overline{mes} \quad (6)$$

$$RB = 100\frac{B}{\overline{mes}} \quad (7)$$

$$IA = 1 - \frac{\sum_{i=1}^{i=N}(mod_i - mes_i)^2}{\sum_{i=1}^{i=N}(|mod_i - \overline{mes}| + |mes_i - \overline{mes}|)^2} \quad (8)$$

where N is the number of data in the discretised series, mes_i and mod_i represent the two sets of measured and simulated values and $\bar{x}$ is the averaged value of the variable x.

The indicator errors for the depth-averaged current are listed in Table 2. An overall good agreement is found between observations and model predictions either in terms of magnitude or direction. As regards the velocity magnitude, the mean index of agreement is 0.983, which indicates very good model performance. A fit of lower quality between model predictions and measurements is obtained at the location of ADCP n°1 (IA = 0.962) which is located Northwest along a series of shoals with minimum depth of around 10 m (Figure 1). This is due to the inability of the RANS model to mimic the turbulent processes triggered by the shoals located south of the ADCP. Indeed, the ADCP signal shows large velocity fluctuations indicating that complex turbulent processes affect the hydrodynamics during the flood tide (when the flow passes over the shoals before reaching the ADCP).

The modelled depth-averaged velocities slightly underestimate the measurements (RB = -2%). However, the depth-averaging of ADCP data is biased by the fact that measurements are not available, neither near the bottom due to the ADCP's blanking distance (in a 3 m-height zone above the seabed), nor near the surface due to side lobe interference. To remove the doubt as regards the bias caused by the depth-averaging of measurements, the horizontal velocities predicted by the model were compared to the measurements at different heights above the seabed: 5, 10, 15, 20 and 30 m. The results, given in Table 3, show that the errors (both the bias and the root mean square error) are independent of the distance from the seabed. The errors vary from an ADCP location to another. Similarly to the results obtained with the depth-averaged velocities, the root mean square error are greater for ADCP n°1 (RMSE = 0.25 m/s) than for the other ADCPs (RMSE < 0.20 m/s). In terms of bias, the velocity magnitude are underestimated at ADCP n° 1 and 3 and overestimated at ADCP n° 2, 4 and 5. However, the bias averaged over the five ADCP locations and over the different heights is very small (-0.05%). Those results confirm the ability of the model to represent accurately the vertical distribution of the velocity. The good model performance is also highlighted in Figure 3 where the modelled and measured velocity profiles are in fairly good agreement at the location of ADCP n°5. Figure 4 displays time series of horizontal velocity and power density extracted 15 m above the seabed, a typical value of hub height (this hub height is used for the simulations with the turbines, section III). At this ADCP location (ADCP n°5), the RMSE in power density is 1.17 kW/m^2 and the RB is 2%. At the ADCPs n° 1, 3 and 4, both the RMSE in power density and the RB at the hub height are less good: 1.31, 1.42, 1.58 kW/m^2 and -10, -8, 13%, respectively. Finally, at the ADCP n°2, the RMSE is very low (0.68 kW/m^2) but the bias is relatively high (RB = 8 %). As expected, the errors in the power density are greater than the errors in velocity

magnitude (because the variable is cubed). However, the errors in power density remain acceptable, especially at the location of ADCP n°5.

Table 2: Performance indicators for the depth-averaged velocities.

ADCP n°	RMSE [m/s]	RB [%]	IA Norm [ ]	RMSE Dir [°]	B [°]
1	0.26	-8	0.962	68	-7
2	0.15	-1	0.986	35	-6
3	0.16	1	0.990	23	10
4	0.17	-1	0.989	22	-4
5	0.17	-0	0.990	22	2

Table 3: RMS errors and relative bias for the horizontal velocities at different heights above the seabed. The NaN value indicates that the proxy cannot be calculated because the depth is insufficient.

ADCP n°	RMSE at 5m [%]	RMSE at 10m [%]	RMSE at 15m [%]	RMSE at 20m [%]	RMSE at 30m [%]
1	0.23	0.25	0.25	0.25	NaN
2	0.18	0.18	0.18	0.18	0.17
3	0.18	0.18	0.19	0.19	0.21
4	0.20	0.21	0.20	0.19	0.20
5	0.16	0.17	0.17	0.17	0.17

ADCP n°	RB at 5m [%]	RB at 10m [%]	RB at 15m [%]	RB at 20m [%]	RB at 30m [%]
1	-5	-6	-6	-8	NaN
2	8	5	5	4	3
3	-1	-1	-3	-4	-5
4	1	2	2	1	1
5	-2	1	1	2	3

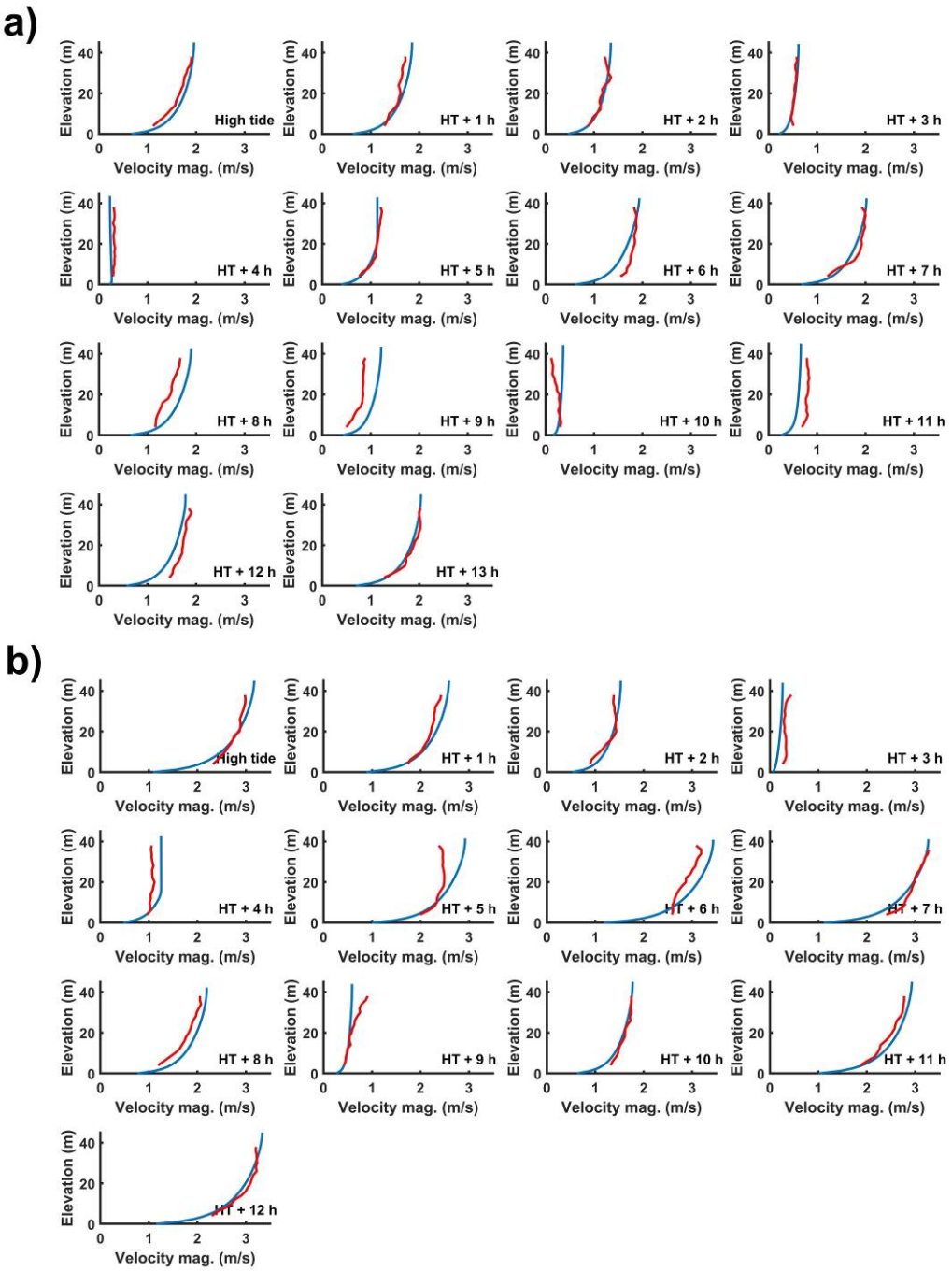

Figure 3: Comparison of the vertical profiles of horizontal velocities at the location of ADCP n°5 during a tide. Blue and red curves represent model results and measurements respectively. In the direction of reading, the profiles are given every hour (the first profile corresponds to high tide). a) Neap tide; b) Spring tide.

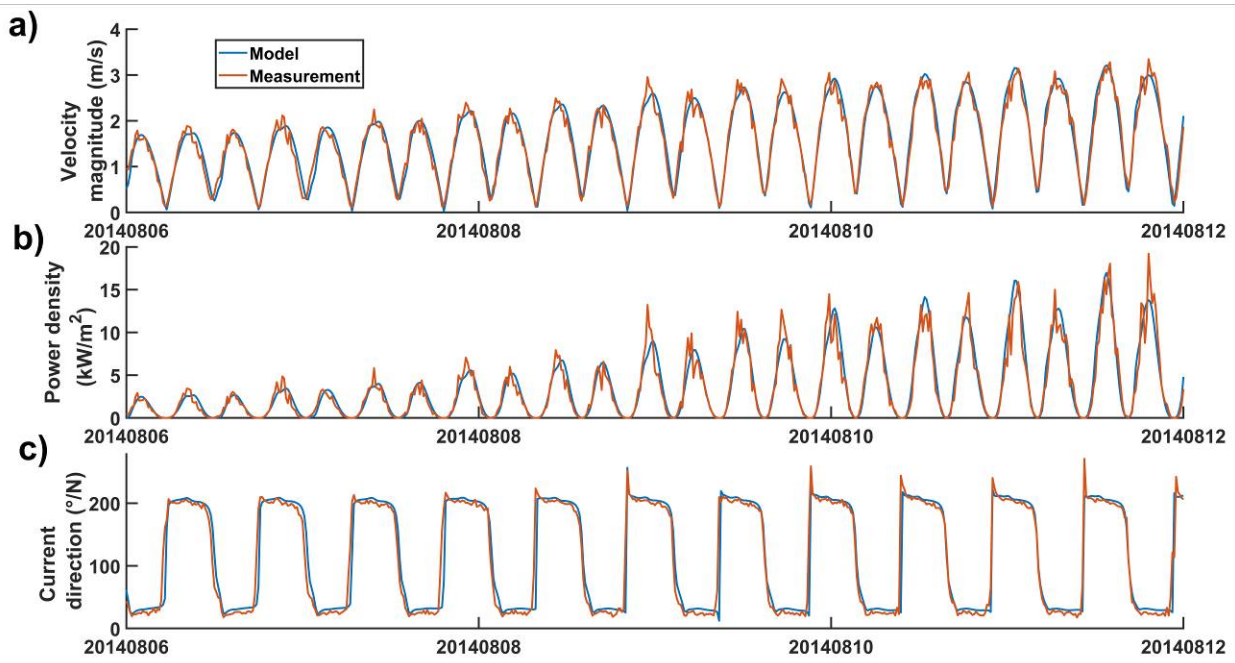

Figure 4: Time-series of horizontal current magnitude (a), power density (b) and current direction at the hub height (c). The data were extracted at the location of ADCP n°5.

III. METHOD FOR THE WAKE FIELD STUDY

A. TURBINE REPRESENTATION

The turbine representation, based on the AD theory, consists in applying a force per unit of volume (Eq. 9) in the area swept by the blades of the turbine. Here, the formulation of Harrison *et al.* (2010) and Nguyen *et al.* (2016) is used. It was implemented in Telemac3D by Thiébot *et al.* (2016). The implementation was validated with the experiments of Myers and Bahaj (2010) that consisted in analyzing the flow field around a tidal turbine represented by a scale mesh disk.

The force per unit of volume (Eq. 9) imposed in the disk derives from the definition of the thrust (Eq. 10), but it is expressed as a function of the local velocity $\vec{u}_{local}$ instead of the upstream (unperturbed) velocity $\vec{u}_{\infty}$, introducing a resistance coefficient K as a function of the thrust coefficient C_T (Eq. 11) (Taylor, 1963, Harrison *et al.*, 2010). This formulation does not include a blockage correction. This simplification is retained here because Chen and Liou (2010) and Kolekar and Banerjee (2015) demonstrated that the correction is not necessary when the blockage ratio is smaller than 10%, which is the case in the following wake-field study.

$$\vec{f} = -\frac{1}{2}\frac{\rho K}{T_{Disk}}\|\vec{u}_{local}\|\vec{u}_{local} \quad (9)$$

$$\vec{f} = -\frac{1}{2}\frac{\rho C_T}{T_{Disk}}\|\vec{u}_{\infty}\|\vec{u}_{\infty} \quad (10)$$

$$C_T = \frac{K}{(1+0.25K)^2} \quad (11)$$

where T_{Disk} is the thickness of the disk, $\|\vec{u}_{local}\|$ is the magnitude of the local velocity $\vec{u}_{local}$ and $\|\vec{u}_{\infty}\|$ is the magnitude of the upstream velocity $\vec{u}_{\infty}$.

The generation of turbulence in the near wake of tidal turbines is induced by (i) the swirl, (ii) the transient characteristics of the flow and (iii) the vortices shed from the blades and the support structure. Those processes, not replicated by the AD, have to be modelled as precisely as possible. Different tuning of turbulence models for AD have been proposed in the literature (*e.g.*, Nguyen *et al.*, 2016, Shives and Crawford, 2017). The tuning of the turbulence model requires experimental data acquired in the wake of a turbine. Such data exist at the laboratory scale but are not available in the wake of a real (full-scale) device. In absence of measurements enabling to tune and validate the turbulence model for the full-scale application, the decision is made to use the k-ε turbulence model without adding any source/sink terms into the AD. This choice relies on earlier works showing that this formulation produces a realistic amount of turbulent kinetic energy when the fluid passes through the AD (Nguyen *et al.*, 2016). This has been furthermore confirmed by Thiébot *et al.* (2016) who compared the velocity and the turbulent intensity predicted by the Telemac3D-AD model to measurements in the wake of porous disk representing a tidal turbine (Myers and Bahaj, 2010).

B. SCENARIOS OF TIDAL ENERGY EXTRACTION

The objective of this study is to compare a series of scenarios of tidal energy extraction to obtain recommendations as regards the positioning of turbines within the array. To this end, a 280m-long and 210m-wide zone centered on the ADCP n°5 is considered (Figure 1). This area is promising for tidal energy exploitation because the resource is high (as shown in section II) and because the depths are suitable to deploy tidal turbines. The seabed is characterised by slight bathymetric variations (the maximal bathymetry variations are smaller than 1 m over the study zone) and the dimensions of the site (280 m x 210 m) are small in comparison to the coastal length scales. These conditions imply that the hydrodynamic characteristics show reduced spatial variations over the selected area. For the simulations with turbines (section IV), the homogeneity of the resource (power of the fluid) facilitates the isolation of the wake-effects from other processes that may drive the difference in production within the array. The other advantage of the selected zone is that the flow is nearly rectilinear: without significant misalignment, there is no need to use a layout favouring the dominant flow direction, which also simplifies the analysis.

A series of eight turbines layout is considered integrating both staggered (Stag) and aligned (Alig) arrangements with two inter-row spacing values (5D and 10D with D the turbine diameter) and two inter-device (lateral) spacing values (3D and 5D) (Figure 5 and Table 4). A simulation without turbines is also performed so that the resource (power of the fluid) can be computed. Furthermore, a single turbine placed in the centre of the study site is simulated to assess the energy extractable by an isolated turbine (not influenced by wake effects). It should be noted that, as the surface of the array is constant and the spacing is variable, the number and the density of turbines vary in each simulation reaching a maximum of 30 devices (6 rows of 5 turbines in configuration Alig_3_5). Depending on the lateral spacing, the local blockage ratio is 5 % and 8.33 % for lateral spacing of 5D and 3D, respectively. Finally, the global blockage ratio is much smaller than 1%, which indicates that the array is not likely to influence the channel-scale dynamics (Vennell *et al.*, 2015).

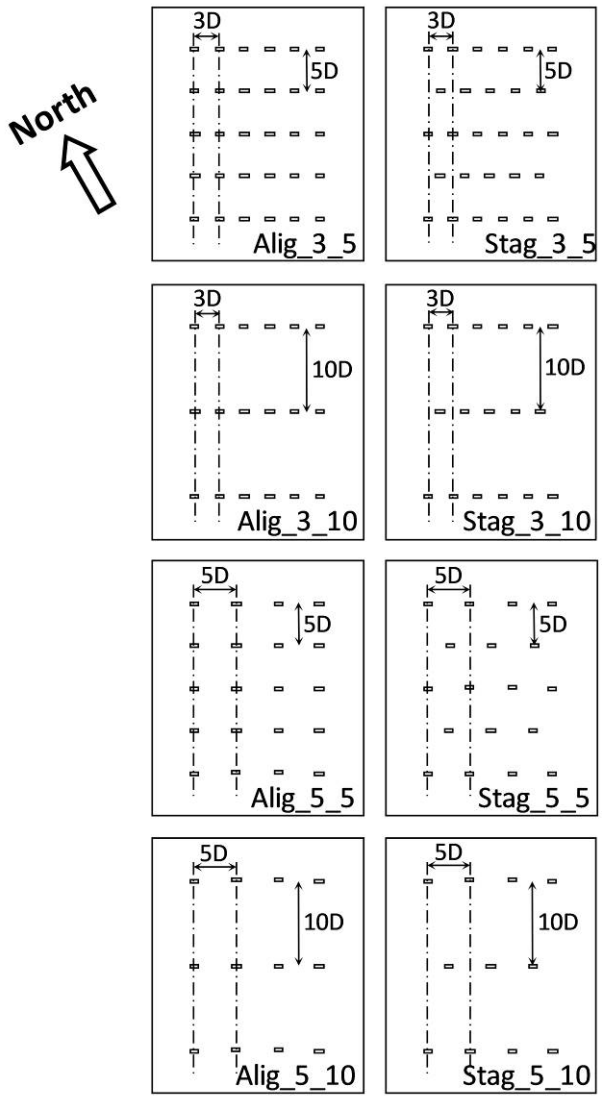

Figure 5: Schematic representations of the layouts.

Table 4: Scenarios of tidal energy extraction.

Name of the run	Type of layout	Lateral spacing (in D)	Longitudinal spacing (in D)	Number of turbines	Local blockage ratio (%)
No turb	-	-	-	0	-
Single	-	-	-	1	-
Stag_3_5	Staggered	3	5	28	8.33
Stag_3_10	Staggered	3	10	17	8.33
Stag_5_5	Staggered	5	5	18	5
Stag_5_10	Staggered	5	10	11	5
Alig_3_5	Aligned	3	5	30	8.33
Alig_3_10	Aligned	3	10	18	8.33
Alig_5_5	Aligned	5	5	20	5
Alig_5_10	Aligned	5	10	12	5

C. FULL-SCALE SIMULATIONS' CHARACTERISTICS

For the simulations with the devices, generic turbine characteristics are retained. The turbine diameter is 14 m and the hub is located 15 m above the seabed. If the upstream velocity is smaller than the cut-in speed, the thrust coefficient C_T is nil. Otherwise, it is constant (Eq. 12). In Eq. 12, the upstream velocity is computed from the local velocity using Eq. 13 (Taylor, 1963, Harrison *et al.*, 2010).

$$\begin{cases} C_T = 0 \;\; if \;\; \|\vec{u}_\infty\| < u_{cutin} \\ C_{T0} \;\; if \;\; u_{cutin} < \|\vec{u}_\infty\| \end{cases} \quad (12)$$

$$\|\vec{u}_\infty\| = \left(1 + \frac{K}{4}\right) \|\vec{u}\| \quad (13)$$

where C_{T0} is set to 0.8 (Bahaj *et al.*, 2007) and u_{cutin} = 1 m/s.

A fixed yaw technology (bi-directional system) is considered because this technology is suited to the study site where the flood and ebb currents are well aligned. Thus, when implementing the AD in Telemac3D, the position of the disks is fixed and the thrust is computed from the axial (local) velocity in Eq. 9. Regional simulations show that the direction maximising the highest and the most frequent cubed velocities values (Thiébot *et al.*, 2016) corresponds to 30° with respect to the North. This value is retained to orientate the turbines (Figure 5).

Prior to integrate ADs in the regional model, a series of tests has been conducted in a 2000m-long, 500m-wide and 40m-deep numerical canal to determine the optimal cell size. Those tests in relation to the convergence of numerical predictions were conducted with hydrodynamic conditions representative of the Alderney Race. At the canal inlet, a 1/7th velocity profile with a maximum velocity of 4 m/s and a turbulent intensity of 10 % is imposed. The convergence of numerical predictions is obtained with a horizontal cell size of 1 m and 40 sigma layers (corresponding to a 1 m vertical spacing between two consecutive planes along the water column). With those settings, each AD contains 5 nodes along the axis of the disk and 140 nodes per cross-section. Thus, each AD contains 700 nodes. Noteworthy, the circular geometry is not exactly represented as a layered mesh is used (the volume within which the thrust is applied is constituted of prismatic elements). However, Thiébot *et al.* (2016) have shown that, with a comparable resolution, the simplification of the turbine geometry does not significantly alter the model predictions in the wake of a single turbine.

For the application to the Alderney Race, the mesh covering the English Channel (Figure 1) has been refined up to 1 m in a 450m-long and 385m-wide zone surrounding the turbines array. The mesh contains 16,843,720 nodes distributed over 40 sigma layers. The time step is set to 0.3 s. The calculation is parallelised over 700 cores (25 sets of 28 cores working at 2.4 GHz with a 128 Go RAM DDR4 - 2400 MHz) resulting in a computational time of the same order of the real time. Finally, mean spring tidal conditions were chosen to obtain results representative of a period with high current magnitude. The model is run between two consecutive high tides. The simulations start twelve hours (one tide) before the aforementioned period to allow the model spin up.

D. FARM/TURBINE PRODUCTION

To analyse the evolution of the global and individual power extracted by the turbines, several proxies are calculated. For a given turbine (numbered *i*), the calculation of the power $P_i(t)$ relies on Eq. 14, where the upstream velocity is computed from the local axial velocity (with Eq. 13).

$$P_i(t) = \frac{1}{nnode}\sum_{j=1}^{nnode}\frac{1}{2}C_P\rho\pi\left(\frac{D}{2}\right)^2\left\|\vec{u}_{\mathrm{i,j},\infty}(t)\right\|^3 \qquad (14)$$

where *nnode* is the number of nodes contained in the AD (those nodes are numbered *j*), D is the turbine diameter and C_P is the power coefficient.

The power output $P_i(t)$ depends on a hypothetical value of power coefficient C_P (set to 0.35 in the present investigation) and on the resource (power of the fluid before extraction). Regional simulations (without turbine) show that the standard deviation of the power at each turbine location is 7 kW, which is 1.3% of the mean value (511 kW). To standardise the comparison between the production of the turbines, the dimensionless production coefficient $DP_i(t)$ is used. It is calculated as the ratio of the turbine output (where the power coefficient is omitted) to the power of the fluid without extraction (Eq. 15).

$$DP_i(t) = \frac{\frac{1}{nnode}\sum_{j=1}^{nnode}\frac{1}{2}\rho\pi\left(\frac{D}{2}\right)^2\left\|\vec{u}_{\mathrm{i,j},\infty}(t)\right\|^3}{\frac{1}{nnode}\sum_{j=1}^{nnode}\frac{1}{2}\rho\pi\left(\frac{D}{2}\right)^2\left\|\vec{u}_{\mathrm{i,j},0}(t)\right\|^3} = \frac{\sum_{j=1}^{nnode}\left\|\vec{u}_{\mathrm{i,j}}(t)\right\|^3}{\sum_{j=1}^{nnode}\left\|\vec{u}_{\mathrm{i,j},0}(t)\right\|^3} \qquad (15)$$

where i is the number of the turbine within the array and $\left\|\vec{u}_{\mathrm{i,j},0}(t)\right\|$ is the magnitude of the velocity computed from the simulation without turbine.

From the calculation of the proxies for individual turbines ($P_i(t)$ or $DP_i(t)$), the global performance of the tidal farm is assessed with $\overline{P(t)} = \sum_{i=1}^{n} P_i(t)/n$ and $\overline{DP(t)} = \sum_{i=1}^{n} DP_i(t)/n$, where n is the number of turbines in the array. To assess the difference of output within the tidal farm, the proxies are computed by row. In this case, the numbering of the row starts from the upstream line (*i.e.* during flood tide, the line n°1 is the line located in the south-western part of the farm; during the ebb tide, the line n°1 is the line located in the north-eastern part of the farm). Finally, when the aforementioned metrics are averaged between two consecutives high tides, they are noted with an index *m*: $\overline{P_m}$ and $\overline{DP_m}$; when they are averaged over the flood or the ebb period, they are noted with an index *flood* or *ebb*: $\overline{P_{flood}}$ or $\overline{P_{ebb}}$.

IV. Results and discussion

A. *Temporal evolution of the output*

Figure 6a illustrates the temporal evolution of the unperturbed velocity magnitude (extracted in the middle of the study zone). It shows that the current magnitude reaches 2.99 m/s during the ebb and 2.81 m/s during the flood (+6% during the ebb). Figure 6b represents the mean production per turbine $\overline{P(t)}$ for different layouts. As the output depends on the cubed velocity, the asymmetry between ebb and flood is exacerbated. The differences between ebb and flood are indicated in Table 5 which synthesises information about the power output. By averaging the results of all layouts, the production is 14% greater during the ebb than during the flood.

The inter-comparison of the output curves (Figure 6b) outlines a high variability in production per turbine from one layout to another. This figure permits thus to identify the layout with the smallest/greatest individual turbine production. The production averaged over a mean spring tidal cycle varies between 211 kW (Alig_3_5) and 303 kW (Stag_5_10). At the time of ebb (resp. flood) peak, the production varies between 573 kW (resp. 388 kW) and 814 kW (resp. 635 kW).

Table 5 also indicates the percentage of time when the turbines are off because the current magnitude is smaller than the cut-in speed. During the selected period, the turbines operate on average 81% of the time.

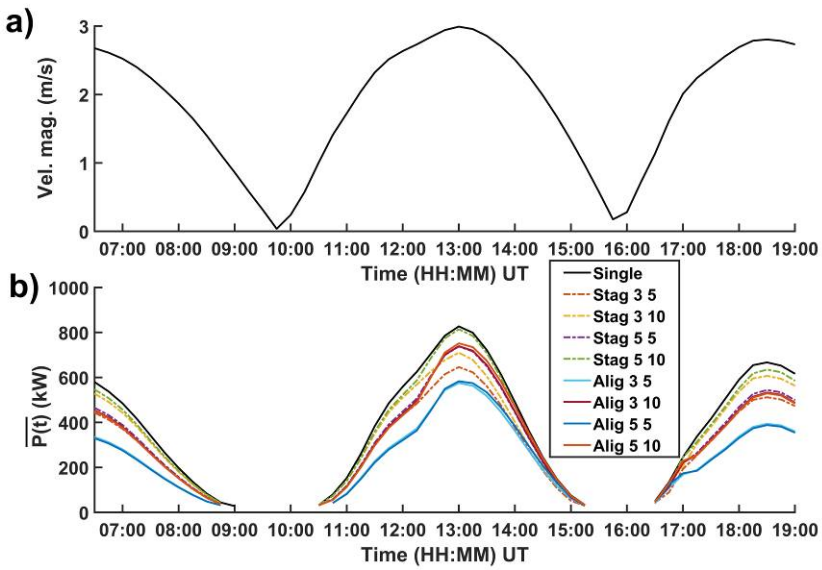

Figure 6: a) Temporal evolution of the velocity magnitude during the selected period. b) Temporal evolution of the output per turbine (total output divided by the number of turbines).

Table 5: Production indicators.

Name of the run	$\overline{P_m}$ (kW)	$\overline{P_{flood}}$ (kW)	$\overline{P_{ebb}}$ (kW)	$\overline{DP_m}$	% of time operation
Single	319	302	338	0.675	82.4
Stag_3_5	252	245	263	0.535	81.0
Stag_3_10	289	282	297	0.612	81.7
Stag_5_5	273	256	293	0.579	81.2
Stag_5_10	303	287	322	0.643	82.2
Alig_3_5	211	194	234	0.448	80.5
Alig_3_10	270	253	291	0.572	81.0
Alig_5_5	213	194	239	0.452	80.5
Alig_5_10	273	252	296	0.577	81.0

B. *Effect of the turbines spacings*

Figure 7 represents the evolution of the farm dimensionless production as a function of the number of turbines. As expected, the isolated turbine exhibits the highest performance with a mean dimensionless production of 0.675. This figure also outlines that, for a comparable density of turbines, the staggered layout produces more than the aligned layout. On average, the output of the staggered turbines is 16% greater than the output of the aligned turbines. As expected, when the turbine density increases, the performance decreases because there is less opportunity for flow recovery between two consecutive rows and more wake superposition. For the more dense arrangements (Stag_3_5 and Alig_3_5), the mean dimensionless production drops to 0.535 and 0.448, respectively. Whether the turbines are staggered or aligned, the layout productions rank as follows: 3D-5D, 5D-5D, 3D-10D, 5D-10D. Whereas the layouts with spacings 5D-5D and 3D-10D have comparable density of turbines (Table 4), the 3D-10D gives a greater output, which suggests that it is preferable to space the turbines along the prevailing current direction.

When the turbines are staggered, reducing the lateral spacing (from 5D to 3D) significantly affects the performance of the layout. The mean loss is -6%. This is an unexpected result because reducing the inter-spacing should theoretically

concentrate the bypass flow and strengthen the production. When the lateral spacing is 3D, the gaps between the turbines is of the same order as the wakes' width. Therefore, the zone of velocity deficit partially overlap the turbines of the next row, especially when the current deviates from the prevailing direction, which reduces their output. This is highlighted in Figure 8a. Noteworthy, a comparable drop of output (when the current is misaligned with the turbines' axis) has already been highlighted in the simulations of Nguyen *et al.* (2019). The other negative effect of reducing the inter-turbine spacing is that it increases the blockage ratio (Table 4) and thus encourages flow diversion around and above the array. The horizontal flow diversion around the array is visible in Figure 8a where the location of the blue and the red zones around the array indicates that the current velocity is reduced upstream of the first row and enhanced on each side of the array. Noteworthy, this flow diversion around the array applies in the same way for the aligned layout (Figure 8b). When the turbines are aligned, reducing the lateral spacing from 5D to 3D has a negligible effect on the dimensionless production of the layout (-1%). This finding suggests that the density of turbines could be further increased (by reducing the inter-turbine spacing) without significant loss of individual production. Figure 8b represents the distribution of the velocity deficit for the Alig_3_5 layout. It shows that the six lines of aligned turbines behave independently (there is no lateral wake overlapping). This may explain why, in the tested conditions, the production is relatively independent of the lateral spacing.

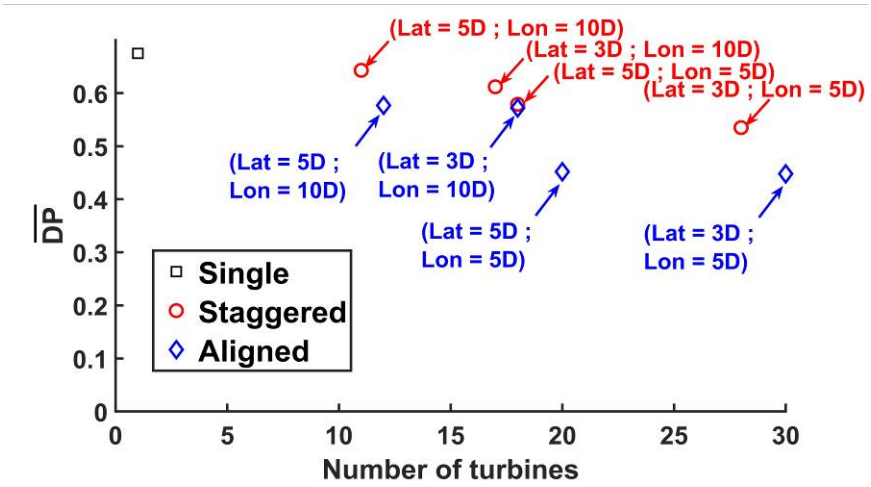

Figure 7: Effect of the number of turbines on the dimensionless production of the array.

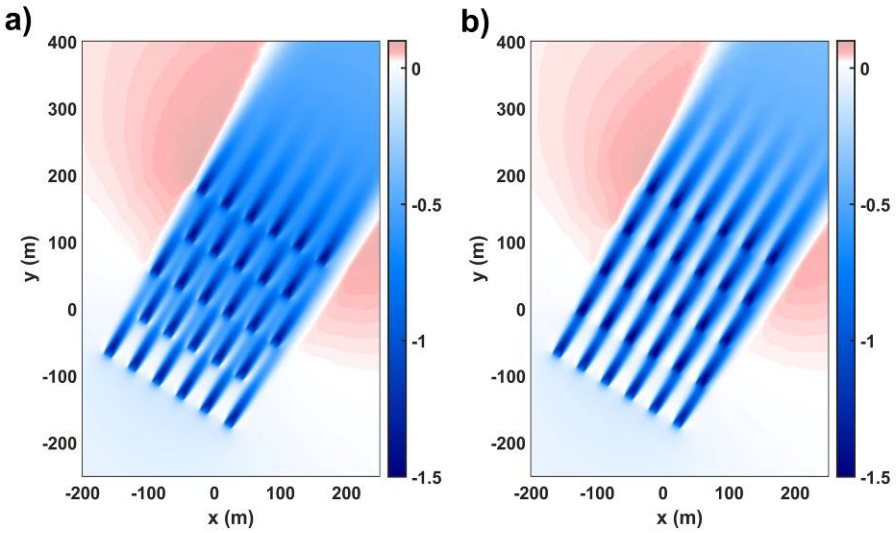

Figure 8: Distribution of the velocity deficit (in m/s) at the time of flood peak. The results are shown in a horizontal plane located at the hub height. a) staggered layout (Stag_3_5); b) aligned layout (Alig_3_5).

C. *Staggered against aligned layout*

Figure 9 presents the dimensionless production of each row. The staggered (continuous lines) and the aligned layouts (dashed lines) clearly behave differently. Before analysing the results, it is recalled that the action of the turbines is based on an AD formulation using a constant thrust coefficient. In other words, no attempts have been made to tune the thrust within the array (such as in Hunter *et al.*, 2015 or Lo Brutto *et al.*, 2017).

For the aligned layout, there is a significant drop of production between the first and the second row. The reason is that the turbines of the second row are located directly in the velocity deficit of the turbines of the first row. Obviously, the drop of production is greater for a longitudinal spacing of 5D than for an inter-row of 10D because the space left for the wake recovery is shorter. However, after the second row, the production experiences reduced variations. This stabilisation of the production is due to the wake-induced turbulence that strongly encourages the flow recovery downstream of the second row of turbine. A similar behaviour has already been highlighted experimentally by Coles *et al.* (2016) who simulated multiple rows of turbines with porous fences. Figures 10b and 11b present the horizontal and vertical distributions of the turbulence intensity within an aligned array. Those figures show that the ambient turbulence is small in comparison to the wake-added turbulence. Between the two first rows, the maximal turbulence intensity is 13% whereas it exceeds 19% between the other rows. This may explain the difference in flow recovery between the two first rows and the other rows.

For the staggered layout, the turbines of a given row are not aligned with those of next row. As the space left for the flow recovery doubles (in comparison to an aligned layout) before reaching the next aligned turbine, the loss of production between two coupled rows (1st and 3rd rows, 2nd and 4th, 3rd and 5th rows) is relatively small. Thus, over the entire array, the loss of production in the stream-wise direction is smaller than with the aligned layout. Figure 9 shows that using a staggered layout avoids a sharp drop of production between the first two rows (as it is obtained with the aligned layout). For the Stag_5_5 layout, there is even a small gain in production between the first and the second row (+1.4%). This is due to the enhancement of the

flow through the gaps between the turbines of the first line. The other process driving the production in the stream-wise direction is the turbulence. As shown in Figures 10a and 11a, the development of the turbulence strongly differs from an aligned to a staggered layout. When the turbines are staggered, there is less wake superposition and more space left for the turbulence to dissipate before reaching another turbine. As the development of turbulence is slower in the stream-wise direction (in comparison to the aligned layout), the beneficial effect of the turbulence on the flow recovery is postponed. This may explain why the flow needs to pass through at least four rows before the production stabilises (Figure 9).

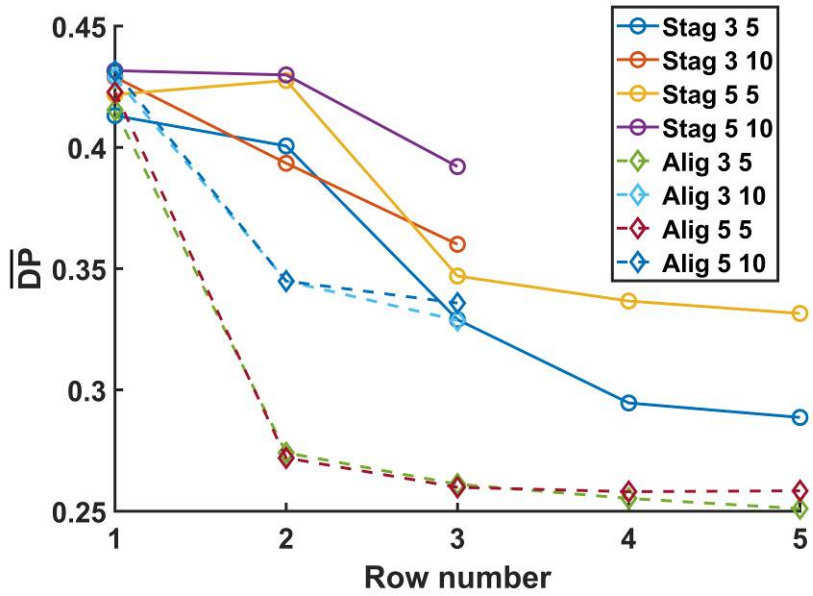

Figure 9: Dimensionless production of each row (in the stream wise direction). The number 1 stands for the row located in the free stream.

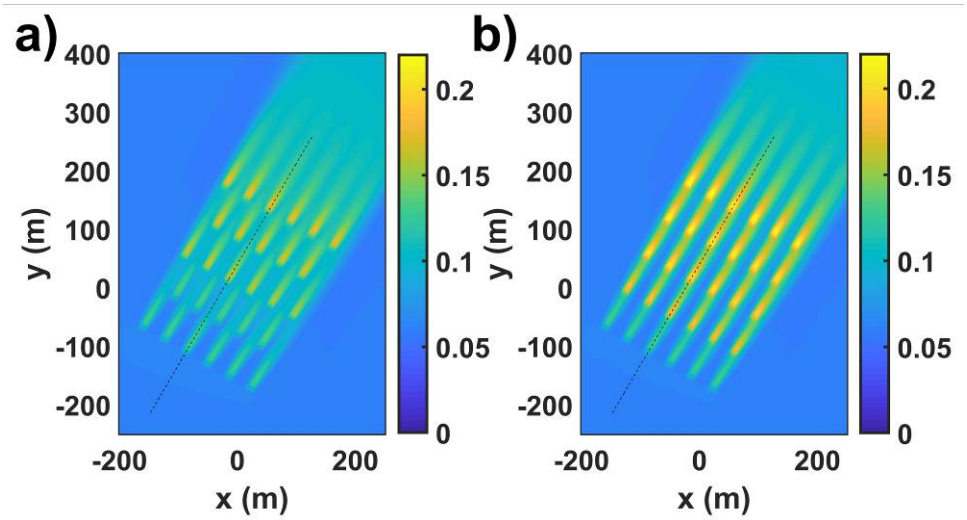

Figure 10: Horizontal distribution of the turbulence intensity (calculated as $\sqrt{(2/3)k}/\|\vec{u}\|$, where k is the turbulent kinetic energy) at the time of flood peak. a) staggered layout (Stag_3_5); b) aligned layout (Alig_3_5). The results are shown in a horizontal plane located at the hub height. The dashed lines indicate the location of the extracted vertical planes represented in Figure 11.

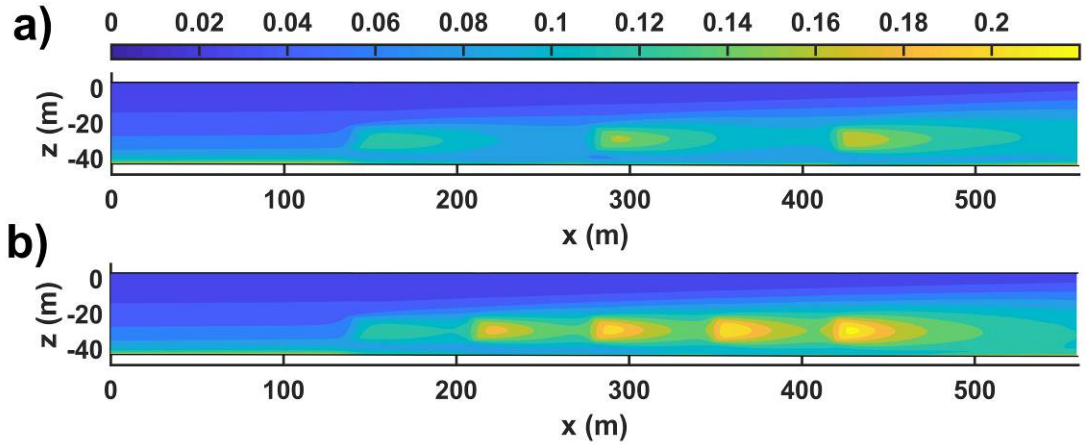

Figure 11: Vertical distribution of the turbulence intensity (calculated as $\sqrt{(2/3)k}/\|\vec{u}\|$, where k is the turbulent kinetic energy) at the time of flood peak. a) staggered layout (Stag_3_5); b) aligned layout (Alig_3_5). The location of the extracted vertical planes is represented in Figure 10.

V. CONCLUSIONS

The primary objective of our study was to assess the efficiency of several tidal turbine arrangements in the Alderney Race. To attain this objective, the small-scale processes have been modelled and only essential physics has been included in the code. Several limitations should therefore be borne in mind.

- Firstly, the comparison of the regional model predictions with the measured current velocities showed that the model accurately reproduces the hydrodynamics of the site under moderate wind and wave conditions. However, there is no guarantee that the model can be applied to more energetic wind/sea conditions. Applying the model to a wider range of meteorological conditions should probably require including the wind and wave effects (and reassessing the model performance considering energetic met-ocean conditions) (*e.g.*, Guillou *et al.*, 2016).
- Secondly, as the ambient turbulence strongly influences the flow recovery, it is important that the model provides reliable turbulence results. In the modelled conditions, the turbulence intensity predicted by the model varies typically between 5 and 15% along a vertical profile. Those values are in line with measurements reported in the scientific literature at comparable sites (*e.g.*, Milne *et al.* 2013). However, the turbulence is site-specific and only a direct comparison with measurements acquired in the Alderney Race would allow validation of the characteristics of the background turbulence predicted by the model. This is clearly beyond the scope of this study.
- Thirdly, our AD implementation only relies on the thrust of the turbine. This AD formulation has already been validated at the laboratory scale (experiments with low blockage ratio). However, for the full-scale application, the required data to tune and validate the AD model (*i.e.* velocity and turbulence intensity measured around and beside a full-scale turbine placed in a real marine environment) are not available. It is therefore important to note that uncertainties remains as regards the characteristics of the wakes predicted by our model. Furthermore, the retained AD formulation does not include a blockage correction (because we restricted the analysis to cases with small blockage ratios). This correction should be included for analyzing configurations with greater blockage ratios (*e.g.*, smaller lateral spacing between turbines or greater turbine diameter

to depth ratio). In this context (cases with greater blockage ratios), the comparison between the efficiency of the different arrangements should be reanalyzed.

By computing both the array and the regional scales, our methodology enables performing a wake field study with realistic tidal flow conditions. The simulations confirm the high potential of the Alderney Race with individual turbine production exceeding 800 kW during spring tides (for a turbine diameter of 14 m and a power coefficient of 0.35). At the study site, the ebb and the flood currents are well aligned and show small directional spreading with respect to the predominant current direction. The asymmetry in production between ebb and flood is of the order of 14% (during spring tides). The comparison of different layouts (staggered and aligned) and different spacings (3D, 5D, 10D) between turbines outlines three main results.

- Firstly, as expected, the longitudinal distance between the rows strongly affects the flow recovery and thus the loss of production in the stream-wise direction. It is clearly advantageous to space the turbines in this direction. When the longitudinal spacing is 10D and when the wake-induced turbulence is well developed, the production experiences however reduced variations between two consecutive rows as the flow recovery, encouraged by the turbulence, is nearly complete.
- Secondly, the lateral spacing has a limited influence on the individual production of the turbines when they are aligned. This implies that the turbines could be deployed close to each other (to gain space). The results suggest that the inter-device spacing could be reduced to less than 3D in the location considered within the Alderney Race. Despite this possible advantage, the aligned layout is unlikely to be more advantageous than the staggered layout. When the turbines are staggered, a minimal lateral spacing of 5D is required to maintain a high efficiency. When this spacing is smaller, the wake overlap and the production drops.
- Thirdly, the results outline significant differences in the spatial distribution of turbulence intensity between the aligned and the staggered layouts. When the turbines are staggered, the wake-induced turbulence develops much more slowly and propagates in a more diffuse way than when the turbines are aligned.

Future work will consist in applying the model at other locations of the Alderney Race where the hydrodynamics is more complex (*e.g.*, misalignment between ebb and flood, more pronounced asymmetry in velocity magnitude, irregular bathymetry…) to obtain more general recommendations as regards the design of arrays in real sites.

ACKNOWLEDGMENT

This work has benefited from a French State support managed by the National Research Agency under the Investments for the Future program bearing the reference ANR-10-IEED-0006-11 (THYMOTE project). We are also grateful to the CRIANN for their help in using their computational resource and to the French navy SHOM ("Service Hydrographique et Océanographique de la Marine") for providing access to bathymetric (HOMONIM project) and sedimentological data (http://data.shom.fr/). The authors warmly thank André Simon (Cerema, DTecEMF/ER/LGCE) for the process of the sedimentological cartography. The present paper is a contribution to the research program DIADEME ("Design et InterActions des Dispositifs d'extraction d'Energies Marines avec l'Environnement") of the Laboratory of Coastal Engineering and Environment (Cerema, http://www.cerema.fr).

REFERENCES

Abolghasemi, M.A., M.D. Piggott, J. Spinneken, A. Viré, C.J. Cotter, S. Crammond, Simulating tidal turbines with multi-scale mesh optimisation techniques. Journal of Fluids and Structures, Volume 66, Pages 69-90, 2016.

Ahmed U., D.D. Apsley, I. Afgan, T. Stallard, P.K. Stansby, Fluctuating loads on a tidal turbine due to velocity shear and turbulence: Comparison of CFD with field data. Renewable Energy, Volume 112, Pages 235-246, 2017.

Bahaj A.S., A.F. Molland, J.R. Chaplin, W.M.J. Batten, Power and thrust measurements of marine current turbines under various hydrodynamic flow conditions in a cavitation tunnel and a towing tank. Renewable Energy, Volume 32, Pages 407-426, 2007.

Bai G., J. Li, P. Fan, G. Li, Numerical investigations of the effects of different arrays on power extractions of horizontal axis tidal current turbines. Renewable Energy, Volume 53, Pages 180-186, 2013.

Batten W.M.J., M.E. Harrison, A.S. Bahaj, Accuracy of the actuator disc-RANS approach for predicting the performance and wake of tidal turbines. Philosophical transactions of the royal society A, 371, 20120293, 2013.

Chen T.Y., L.R. Liou, Blockage correction in wind tunnel test of small horizontal-axis wind turbines. Experimental Thermal and Fluid Science, Volume 35, Pages 565-569, 2011.

Churchfield MJ, Y. Li, P.J. Moriarty, A large-eddy simulation study of wake propagation and power production in an array of tidal-current turbines. Philosophical transactions of the royal society A, 371: 20120421, 2013.

Coles D.S., L.S. Blunden, A.S. Bahaj, Assessment of the energy extraction potential at tidal sites around the Channel Islands. Energy, Volume 124, Pages 171-186, 2017.

Coles D.S., L.S. Blunden, A.S. Bahaj, Experimental validation of the distributed drag method for simulating large marine current turbine arrays using porous fences. International Journal of Marine Energy, Volume 16, Pages 298-316, 2016.

Egbert G.D., S. Y. Erofeeva, R. D. Ray, Assimilation of altimetry data for nonlinear shallow-water tides: quarter-diurnal tides of the Northwest European Shelf. Continental Shelf Research, Volume 30, Pages 668-679, 2010.

Fallon D., M. Hartnett , A. Olbert, S. Nash, The effects of array configuration on the hydro-environmental impacts of tidal turbines. Renewable Energy, Volume 64, Pages 10-25, 2014.

Goward Brown A.J., S.P. Neill, M.J. Lewis, Tidal energy extraction in three-dimensional ocean models. Renewable Energy, Volume 114, Pages 244-257, 2017.

Guillou N., J. Thiébot, The impact of seabed rock roughness on tidal stream power extraction. Energy, Volume 112, Pages 762-773, 2016.

Guillou N., G. Chapalain, S.P. Neill, The influence of waves on the tidal kinetic energy resource at a tidal stream energy site. Applied Energy, Volume 180, Pages 402-415, 2016.

Harrison, M.E., W.M.J. Batten, L.E. Myers, A.S. Bahaj, Comparison between CFD simulations and experiments for predicting the far wake of horizontal axis tidal turbines. IET Renewable Power Generation, Volume 4(6), Pages 613-627, 2010.

Hervouet J.-M., Hydrodynamics of Free Surface Flows, Modelling with the Finite-Element method. John Wiley & Sons Ltd, West Sussex, England, 340 pages, 2007.

Hunter W., T. Nishino, R.H.J. Willden, Investigation of tidal turbine array tuning using 3D Reynolds-Averaged Navier–Stokes Simulations. International Journal of Marine Energy, Volume 10, Pages 39-51, 2015.

Kolekar N., A. Banerjee, Performance characterization and placement of a marine hydrokinetic turbine in a tidal channel under boundary proximity and blockage effects. Applied Energy, Volume 148, Pages 121-133, 2015.

Lo Brutto O.A., S. Guillou, J. Thiébot, H. Gualous, Assessing the effectiveness of a global optimum strategy within a tidal farm for power maximization. Applied Energy, Volume 204, Pages 653-666, 2017.

Liu J., H. Lin, S.R. Purimitla, Wake field studies of tidal current turbines with different numerical methods. Ocean Engineering, Volume 117, Pages 383-397, 2016.

Malki R., I. Masters, A.J. Williams, T.N. Croft, Planning tidal stream turbine array layouts using a coupled blade element momentum - computational fluid dynamics model. Renewable Energy, Volume 63, Pages 46-54, 2014.

Milne I.A., R.N. Sharma, R.G.J. Flay, S. Bickerton, Characteristics of the turbulence in the flow at a tidal stream power site. Philosophical transactions of the royal society A, Volume 371, Pages 1-14, 2013.

Mycek P., Gaurier B., Germain G., Pinon G., Rivoalen E., Experimental study of the turbulence intensity effects on marine current turbines behaviour. Part II: two interacting turbines. Renewable Energy, Volume 68, Pages 876-892, 2014.

Myers L.E., A.S. Bahaj, Experimental analysis of the flow field around horizontal axis tidal turbines by use of scale mesh disk rotor simulators. Ocean Engineering, Volume 37, Pages 218–227, 2010.

Neill S.P., M. R. Hashemi, M.J. Lewis, Tidal energy leasing and tidal phasing. Renewable Energy, Volume 85, Pages 580-587, 2016.

Nguyen V.T., S.S. Guillou, J. Thiébot, A. Santa Cruz, Modelling turbulence with an actuator disk representing a tidal turbine. Renewable Energy, Volume 97, Pages 625-635, 2016.

Nguyen V.T., S.S. Guillou, A. Santa Cruz, M.S.N. Elsouk, J. Thiébot, Effect of a Varying Current Direction on the Energy Production of a Pilot Tidal Farm by a Pseudo Steady Approach. 12th European Wave and Tidal Energy Conference Proceeding, Cork, 28-31 August 2017, #977, 8p.

Nguyen V.T., A. Santa Cruz, S.S. Guillou, M.S.N. Shiekh Elsouk, J. Thiébot, Effects of the current direction on the energy production of a tidal farm: the case of Raz Blanchard (France), Energies, Volume 12, 2478, 20 p., 2019.

O'Hara Murray R., A. Gallego, A modelling study of the tidal stream resource of the Pentland Firth, Scotland. Renewable Energy, Volume 102, Part B, Pages 326-340, 2017.

Peyrard C., C. Buvat, F. Lafon, C. Abonnel, Investigations of the wake effects in marine current farms, through numerical modelling with the TELEMAC system. In: Proceedings of the 1st International Conference on Ocean Energy, Bremerhaven, Germany, 23-24 October 2006.

Roc T., D.C. Conley, D. Greaves, Methodology for tidal turbine representation in ocean circulation model. Renewable Energy, Volume 51, Pages 448-464, 2013.

Roc T., D. Greaves, K.M. Thyng, D.C. Conley. Tidal turbine representation in an ocean circulation model: Towards realistic applications. Ocean Engineering, Volume 78, Pages 95–111, 2014.

Saha S., S. Moorthi, H. Pan, X. Wu, J. Wang, S. Nadiga *et al.* The NCEP climate forecast system reanalysis. Bulletin of the American Meteorological Society, Volume 91, Pages 1015-1057, 2010.

Shives M., C. Crawford, Tuned actuator disk approach for predicting tidal turbine performance with wake interaction. International Journal of Marine Energy, Volume 17, Pages 1–20, 2017.

SHOM, MNT Bathymétrique de façade Atlantique http://dx.doi.org/10.17183/MNT_ATL100m_HOMONIM_WGS84, 2015.

SHOM, http://datashom.fr, 2018.

Soulsby R., The bottom boundary layer of shelf seas. Johns BE. Physical oceanography of coastal and shelf seas. Amsterdam: Elsevier. Pages 189-266, 1983.

Taylor G.I., Air resistance of a flat plate of very porous material. In: The Scientific Papers of Sir Geoffrey Ingram Taylor. Cambridge University Press, 1963, Pages 384-386, 1963.

Thiébot J., P. Bailly du Bois, S. Guillou. Numerical modeling of the effect of tidal stream turbines on the hydrodynamics and the sediment transport - Application to the Alderney Race (Raz Blanchard), France. Renewable Energy, Volume 75, Pages 356-365, 2015.

Thiébot J., S. Guillou, V.T. Nguyen, Modelling the effect of large arrays of tidal turbines with depth-averaged Actuator Disks. Ocean Engineering, Volume 126, Pages 265-275, 2016.

Yang Z., Wang, T, Copping, A.E., Modeling tidal stream energy extraction and its effects on transport processes ina tidal channel and bay system using a three-dimensional coastal ocean model, Renewable Energy, Volume 50, Pages 605-6013, 2013.

Yang Z., Wang, T, Copping, A.E., Array optimization for tidal energy extraction in a tidal channel – A numerical modelling analysis. Proceedings of the 2nd Marine Energy Technology Symposium METS2014 April 15-18, 2014, Seattle, WA. 5p.

Weilbeer H., J.A. Jankowski, A Three-Dimensional Non-Hydrostatic Model for Free Surface Flows - Development, Verification and Limitations. Estuarine and Coastal Modeling. Proceedings of the 6th International Conference, ASCE, 1999.